Aalborg Universitet

Adaptive fuzzy sliding mode algorithm-based decentralised control for a permanent magnet spherical actuator

Liu, Jingmeng; Li, Xuerong; Cai, Shaoxiong ; Chen, Weihei; Bai, Shaoping

Adaptive fuzzy sliding mode algorithm-based decentralised control for a permanent magnet spherical actuator

Jingmeng Liu, Xuerong Li, Shaoxiong Cai, Weihai Chen & Shaoping Bai

View supplementary material

Published online: 11 Dec 2018.

Submit your article to this journal

View Crossmark data

Taylor & Francis
Taylor & Francis Group

Check for updates

Adaptive fuzzy sliding mode algorithm-based decentralised control for a permanent magnet spherical actuator

Jingmeng Liu[a], Xuerong Li[a], Shaoxiong Cai[a], Weihai Chen[a] and Shaoping Bai[b]

[a]School of Automation Science and Electrical Engineering, Beihang University, Beijing, People's Republic of China; [b]Department of Materials and Production, Aalborg University, Aalborg, Denmark

ABSTRACT

The dynamic model of multi-degree-of-freedom permanent magnet (PM) spherical actuators is multivariate and nonlinear due to strong inter-axis couplings, which affects the trajectory tracking performance of the system. In this paper, a decentralised control strategy based on adaptive fuzzy sliding mode (AFSM) algorithm is developed for a PM spherical actuator to enhance its trajectory tracking performance. In this algorithm, the coupling terms are separated as subsystems from the entire system. The AFSM algorithm is applied in such a way that the fuzzy logic systems are used to approximate the subsystem with uncertainties. A sliding mode term is introduced to compensate for the effect of coupling terms and fuzzy approximation error. The stability of the proposed method is guaranteed by choosing the appropriate Lyapunov function. Both simulation and experimental results show that the proposed control algorithm can effectively handle various uncertainties and inter-axis couplings, and improve the trajectory tracking precision of the spherical actuator.

1. Introduction

Multiple degree-of-freedom (DOF) actuators have wide potential applications such as robot manipulators, automobile wheels, vision systems and precision assemblings. Conventionally, multiple-DOF actuators are implemented by combining several single-axis motors which have inevitable disadvantages such as complex structure, large backlash and slow response. As an alternative, spherical actuators which can realise 3-DOF motion in one single joint are advantageous due to simple mechanical structure and rapid response. So far, various structures and working principles of 3-DOF spherical actuators have been proposed, such as spherical ultrasonic motors (Toyama & Kobayashi, 1996), spherical induction actuators (Dehez et al., 2002) and permanent magnet (PM) spherical actuators. In this paper, our interest is the PM spherical actuators. In past years, this type of actuator has been studied, which reveals their advantages of small volume, high flux density (Hey, Teo, Bui, Yang, & Martinez-Botas, 2014; Shigeki, Shigeru, Zhang, & Yasutaro, 1995; Takahara, Hirata, Niguchi, Nishiura, & Sakaidani, 2017; Yan, Chen, Lim, Yang, & Lee, 2011).

Many control algorithms have been proposed for PM spherical actuators to achieve high trajectory tracking performance. A typical method to control PM spherical actuator is to use proportional-derivative (PD) control law (Jia, 2003; Maeda, Hirata, Ikejiri, & Tong, 2010; Wang, Wang, Jewell, & Howe, 2003; Xia, Song, Li, Li, & Shi, 2009). However, the dynamic model of PM spherical actuator includes nonlinearities, uncertainties and strong inter-axis couplings among various inputs and outputs (Son & Lee, 2010), and the trajectory tracking performances will be seriously affected with the PD control scheme. To compensate for the nonlinearities and couplings, a computed torque method has been used (Bai & Lee, 2014; Chen, Zhang, Yan, & Liu, 2012; Son & Lee, 2014). It can linearise and decouple the dynamics of the spherical actuator, whereas it cannot achieve a high trajectory tracking performance especially in the presence of various external disturbances. To cope with these problems, the neural networks control is applied due to their learning ability and adaptation (Chu, Niguchi, & Hirata, 2013; Yan et al., 2017; Jia, 2000). However, the neural networks control required considerable computational time and extensive training data, which brings challenge to real-time control. Meanwhile, a robust control scheme which combines the backstepping and sliding mode control method has been implemented for PM spherical actuators with modelling errors and external disturbances (Liu, Deng, Hu, Hua, & Chen, 2017). As this method does not take the decoupling terms into consideration, the tracking accuracy improvement is limited. In

Liu, Deng, Chen, and Bai (2017), an active disturbance rejection control is developed to reformulate the decoupling problems as disturbance rejection by merging the cross channel interference into lumped disturbance. Nevertheless, the selection of parameters and nonlinear functions is a natural challenge which limits its application in practice.

In recent years, advanced control strategies are developed for systems with interconnections, nonlinearities, or uncertainties (Li, Liu, Chen, & Bai, 2018; Utkin, Guldner, & Shi, 2009). Decentralised control strategy arises from various complex situations where there exist coupling terms among several subsystems (Ma, Na, & Zhong, 2013; Wang & Lin, 2015; Wang, Liu, Qiu, & Liu, 2017). Adaptive fuzzy control has been successfully used in nonlinear systems with partially unknown functions (Chen, Lin, Liu, & Liu, 2016; Zhou, Li, Wu, Wang, & Ahn, 2017). Due to its approximation property, fuzzy control can be used for approximating unknown dynamics with a satisfactory tracking results, which has been applied to the identification analysis and design of control systems (Chen, Liu, Ge, & Lin, 2012; Feng, 2006). Recently, variable structure control algorithm based on the sliding mode has been successfully used in the field of industrial robots, as it is insensitive to parameter variations, disturbances and noise (Bartolini, Levant, Pisano, & Usai, 2016; Fei & Lu, 2018). Hybrid control schemes which combine the advantages of different methods are also developed (Shen, Shi, & Shi, 2016; Zheng, Wu, Xu, & Chen, 2015). An adaptive backstepping fuzzy sliding mode control is introduced by combining the backstepping method with adaptive fuzzy control to approximate the unknown system dynamics (Fang, Fei, & Hu, 2018). A decentralised adaptive fuzzy sliding mode (AFSM) control is proposed for reconfigurable modular manipulators with guaranteed stability and trajectory tracking performance (Zhu & Li, 2010). The dynamics of PM spherical actuator is a nonlinear system with strong couplings, modelling errors and external disturbances, therefore it is desirable to combine the advantages of those control methods to obtain a new hybrid control scheme in order to significantly improve its performance.

The motivation of this work is to develop a hybrid control strategy which can linearise and decouple the nonlinear dynamic model of PM spherical actuators and has the ability to compensate for various uncertainties in real-time control. This paper presents a decentralised control strategy based on the AFSM for the complex dynamic model of the PM spherical actuator. It's a hybrid control strategy which combines the advantages of decentralised control, adaptive fuzzy algorithm and sliding mode control: (1) The decentralised control can decouple the dynamic model by separating terms only depending on local variables from other variables, which can avoid difficulties in complexity of controller design; (2) The fuzzy control is used to approximate the subsystems of the dynamic model to remove the effect of uncertainties including the modelling errors and external disturbances, which means the precise knowledge of entire dynamic model is not required; (3) The sliding mode controller is used to remove the effect of coupling terms and compensate for the errors of fuzzy approximation; (4) An adaptive law is employed to update the control parameters online which ensure the effectiveness and robustness of the controller. In contrast to previous works, this hybrid control method takes multiple issues of PM spherical actuators into considerations simultaneously to improve the accuracy of the trajectory tracking performance.

The paper is organised as follows. Section 2 presents the dynamic and torque models of a PM spherical actuator. Section 3 reformulates the nonlinear dynamic model with interconnections and uncertainties by introducing the decentralised control, and illustrates the design of AFSM controller. The stability of the closed-loop system is proved in that section. Sections 4 and 5 present the results of simulations and experiments, respectively. The concluding remarks are finally given in Section 6.

2. PM spherical actuator

The mechanical structure of the PM spherical actuator is shown in Figure 1. The PM spherical actuator mainly consists of a ball-shaped rotor with 16 PM poles arranged in two layers along the equatorial plane and 36 air-core coils distributed in three layers symmetrically about the equatorial plane of the stator. The rotor is supported by a passive spherical joint which includes a rotary encoder and two potentiometers to measure the orientation of the rotor for closed-loop system. Additionally, this joint also acts as the support of the rotor for achieving 3-DOF motion within a confined workspace.

Figure 2(a ,b) show the working principle of spinning motion and tilting motion generated by the attraction or repulsion forces between the coils and PMs. Specifically, with pairs of coils activated in two longitudinal directions, the rotor can realise tilting motion in two longitudinal directions, while the spinning motion is governed by energising all the circumferential coils in order. The rotor can produce corresponding motion within the workspace by activating the input currents of stator coils in a specific approach.

2.1. Dynamic modelling

The spherical joint mechanism is comprised of a 1-DOF passive rotary joint in conjunction with a 2-DOF passive
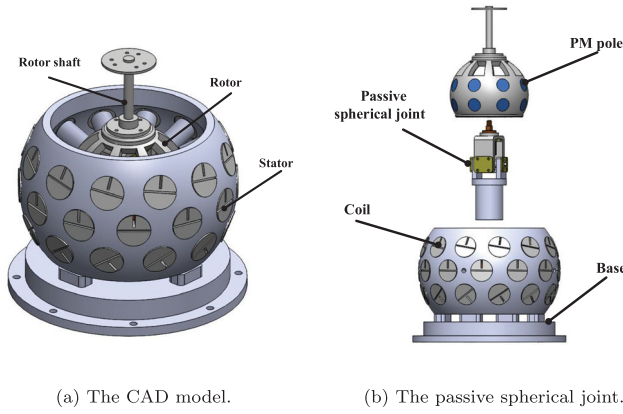
(a) The CAD model.　　(b) The passive spherical joint.

Figure 1. Concept of PM spherical actuator. (a) The CAD model and (b) the passive spherical joint.

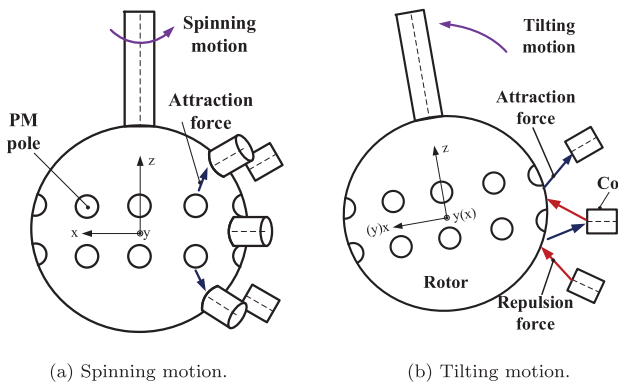(a) Spinning motion.　　(b) Tilting motion.

Figure 2. The 3-DOF motion of PM spherical actuator. (a) Spinning motion and (b) tilting motion.

universal joint. It can be decomposed into three serially connected 1-DOF revolute joints perpendicular to each other (see Figure 3(a)). The rotation angle of each revolute joint is detected by the sensors installed in the spherical joint. There is a 3-DOF rigid-body rotational motion between the stator and rotor. Figure 3(b) shows the coordinate transformation from the rotor frame T_R to the stator frame T_S coordinate system. The rotation matrix R_{rs} is an orthogonal matrix given by:

$$R_{rs} = \begin{bmatrix} c\beta c\gamma & -c\beta s\gamma & s\beta \\ c\gamma s\alpha s\beta + c\alpha s\gamma & c\alpha c\gamma - s\alpha s\beta s\gamma & -c\beta s\alpha \\ -c\gamma s\alpha s\beta + s\alpha s\gamma & c\gamma s\alpha + c\alpha s\beta s\gamma & c\alpha c\beta \end{bmatrix},$$

where c and s represent cosine and sine, respectively. XYZ Euler angles (α, β, γ) are used here to describe the orientation of the rotor (Murray, Sastry, & Li, 1994). It can provide a mapping between the rotor orientation and rotation angles of three revolute joints. It is noted that the orientation can also be expressed with Euler parameters (Bai, Hansen, & Andersen, 2009). In this work, we adopt Euler angles to describe the motor rotations (Figure 2).
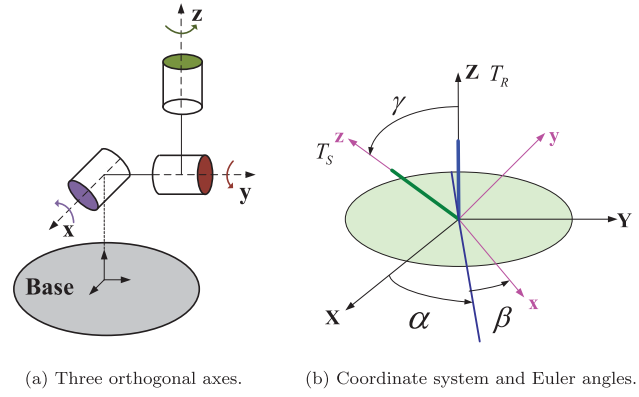

(a) Three orthogonal axes.　　(b) Coordinate system and Euler angles.

Figure 3. Kinematics of PM spherical actuator. (a) Three orthogonal axes and (b) coordinate system and Euler angles.

The ideal dynamic model of the PM spherical actuator can be derived using the Lagrange equation as follows:

$$M(q)\ddot{q} + C(q, \dot{q})\dot{q} + G(q, \dot{q}) = \tau_c - \tau_l - \tau_r = \tau_c - \tau_d, \tag{1}$$

where $M(q)$ is the inertial matrix; $C(q, \dot{q})$ and $G(q, \dot{q})$ represent the Coriolis and gravity matrix terms, respectively. $q = [\alpha, \beta, \gamma]^T$ denotes the vector of the Euler angles; $\tau_c = [\tau_\alpha \ \tau_\beta \ \tau_\gamma]^T$ is the vector of control torques; $\tau_d = \tau_l + \tau_r$ denotes the disturbances which include the external disturbance τ_r and load torque τ_l. The principal inertial moments of the rotor are $J_1 = J_{xx} = 2.219 \times 10^{-3}(\text{kg m}^2)$, $J_2 = J_{yy} = 2.176 \times 10^{-3}(\text{kg m}^2)$, $J_3 = J_{zz} = 2.256 \times 10^{-3} \ (\text{kg m}^2)$. Specifically, M is given as follows:

$$M = \begin{bmatrix} J_1 c^2\beta c^2\gamma + J_2 c^2\beta s^2\gamma \\ +J_3 s^2\beta & (J_1 - J_2)c\beta c\gamma s\gamma & J_3 s\beta \\ (J_1 - J_2)c\beta c\gamma s\gamma & J_1 s^2\gamma + J_2 c^2\gamma & 0 \\ J_3 s\beta & 0 & J_3 \end{bmatrix}$$

and the gravity term in Equation (1) is:

$$G(q, \dot{q}) = \mathbf{0}. \tag{2}$$

The details of Coriolis matrix are described in the appendix. To analyse the inter-axis coupling effect of the PM spherical actuator, it's assumed that $J_1 = J_2 = J_3 = J$ in inertial and Coriolis matrix. The dynamic model can be simplified as follows:

$$J\ddot{\alpha} + Js(\beta)\ddot{\gamma} + Jc(\beta)\dot{\beta}\dot{\gamma} = \tau_\alpha - \tau_{d1}, \tag{3}$$

$$J\ddot{\beta} - Jc(\beta)\dot{\alpha}\dot{\gamma} = \tau_\beta - \tau_{d2}, \tag{4}$$

$$Js(\beta)\ddot{\alpha} + J\ddot{\gamma} + Jc(\beta)\dot{\alpha}\dot{\beta} = \tau_\gamma - \tau_{d3}. \tag{5}$$

The equivalent coupling torques on α-axis are

$$\tau_{\alpha1} = Js(\beta)\ddot{\gamma}, \tag{6}$$

$$\tau_{\alpha 2} = Jc(\beta)\dot{\beta}\dot{\gamma}, \tag{7}$$

where $\tau_{\alpha 1}$ is the inertial coupling term and $\tau_{\alpha 2}$ is the Coriolis force term. The equivalent coupling torque on β-axis is

$$\tau_{\beta 1} = -Jc(\beta)\dot{\alpha}\dot{\gamma}, \tag{8}$$

where $\tau_{\beta 1}$ is the Coriolis force term. The equivalent coupling torques on γ-axis are

$$\tau_{\gamma 1} = Js(\beta)\ddot{\alpha}, \tag{9}$$

$$\tau_{\gamma 2} = Jc(\beta)\dot{\alpha}\dot{\beta}, \tag{10}$$

where $\tau_{\gamma 1}$ is the inertial coupling term and $\tau_{\gamma 2}$ is the Coriolis force term. It can be seen from Equations (3)–(5) that the dynamic model has nonlinear characteristics, and many inter-axis coupling terms exist in the dynamic model.

Note that modelling errors cannot be avoided due to the complexity of the real physical system. Considering the effects of the dynamic modelling uncertainties, the dynamic model can be shown to satisfy:

$$\hat{M}(q)\ddot{q} + \hat{C}(q,\dot{q})\dot{q} + \hat{G}(q,\dot{q}) = \tau_c - \tau_d, \tag{11}$$

where $\hat{M}(q) = M(q) + \Delta M(q)$ is the actual inertial matrix; $\hat{C}(q,\dot{q}) = C(q,\dot{q}) + \Delta C(q,\dot{q})$ is the actual Coriolis matrix; $\hat{G}(q,\dot{q}) = G(q,\dot{q}) + \Delta G(q,\dot{q})$ is the actual gravity matrix; $\Delta M(q), \Delta C(q,\dot{q}), \Delta G(q,\dot{q})$ are the modelling errors.

2.2. Torque modelling

The driving torque of the PM spherical actuator is determined by the coil currents and the rotor orientation. The coils of proposed spherical actuator are wound on non-ferromagnetic cores, thus the torque output is proportional to the current input. The complete torque model can be derived by using the superposition principle. The finite element analysis is used to obtain the torque generated by one coil and the PM array of rotor with different separation angles. The numerical model is built in Ansoft 3D as shown in Figure 4(a). In the model, the iron hoop is used for mounting the PM poles, and the air gap between the rotor and stator is 0.5 mm.

Since the air-core coils are used in PM spherical actuator, the torque varies linearly with respect to the current inputs. The torque model can be obtained by summing up the torques generated by all the coils (Lim, Chen, Yan, Yang, & Lee, 2009). The total control torque τ_c of the PM spherical actuator can be expressed as:

$$\tau_c = [\tau_x \quad \tau_y \quad \tau_z]^{\mathrm{T}} = G_t I, \tag{12}$$

where G_t is the torque matrix which is described as:

$$G_t = [G_{t1} \quad \cdots \quad G_{tj} \quad \cdots G_{tN}], \quad G_{tj} \in R^{3 \times 1} \tag{13}$$

and I is the vector of current inputs of the stator coils:

$$I = [I_1 \quad \cdots \quad I_j \quad \cdots \quad I_N]^{\mathrm{T}} \tag{14}$$

herein, N is the number of stator coil groups; G_{tj} is the torque coefficient, which describes the torque contribution of the jth coil with 16 PMs at a specific rotor orientation; I_j is the current input of the jth coil. G_{tj} is given as:

$$G_{tj} = \begin{cases} \sum_{i=1}^{16} (-1)^{i-1} f_t(\varphi_{ij}) \\ \quad (r_i \times s_j / |r_i \times s_j|), & r_i \times s_j \neq 0, \\ 0, & r_i \times s_j = 0, \end{cases} \tag{15}$$

where $f_t(\varphi_{ij})$ is a torque function between the ith PM pole and the jth coil obtained by curve fitting of the computed data using a finite element (FE) method (see Figure 4(b)) and $\varphi_{ij} = \cos^{-1}(r_i, s_j)$ is the separation angle between the ith PM pole and the jth coil.
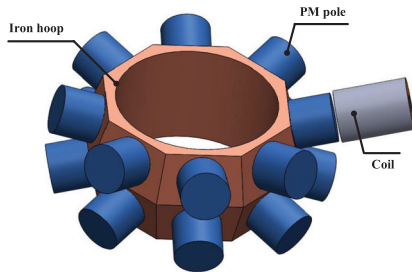
(a) Finite element model.
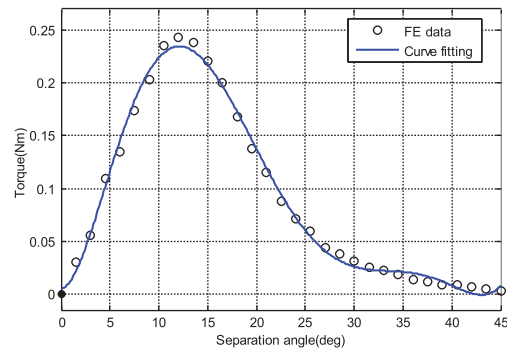
(b) Curve fit of the FE.

Figure 4. Torque between a PM pole and a coil. (a) FE model and (b) curve fit of the FE.

Given desired control torque τ_c at a specific rotor orientation, the currents of the coils I are calculated as (Zhang, Chen, Yan, & Liu, 2011):

$$I = G_t{}^{\mathrm{T}}(G_t G_t{}^{\mathrm{T}})^{-1}\tau_c. \qquad (16)$$

It should be noted that all the coils are divided into 18 groups, and the coils whose axes are collinear are arranged into one group.

3. AFSM algorithm-based decentralised control

3.1. Reformulation of decentralised control problem

The nonlinear dynamics of the PM spherical actuator with uncertainties and cross-couplings is clearly shown in Equation (11). In the literatures of the decentralised control, such a multiple-input multiple-output (MIMO) system can be partition into three single-input single-output (SISO) subsystems which are dependent from each other (Wang et al., 2017). By separating terms depending on only local variables $(q_i, \dot{q}_i, \ddot{q}_i)$ from those terms of other variables, each subsystem of the dynamic model can be reformulated as (Tang, Tomizuka, Guerrero, & Montemayor, 2000):

$$\hat{M}_i(q_i)\ddot{q}_i + \hat{C}_i(q_i, \dot{q}_i)\dot{q}_i + \hat{G}_i(q_i, \dot{q}_i)$$
$$+ Z_i(q, \dot{q}, \ddot{q}) = \tau_{ic} - \tau_{id} \qquad (17)$$

with

$$Z_i(q, \dot{q}, \ddot{q}) = \left\{ \sum_{j=1, i\neq j}^{n} \hat{M}_{ij}(q)\ddot{q}_j + [\hat{M}_{ii}(q) - \hat{M}_i(q_i)]\ddot{q}_i \right\}$$
$$+ \left\{ \sum_{j=1, i\neq j}^{n} \hat{C}_{ij}(q, \dot{q})\dot{q}_j \right.$$
$$\left. + [\hat{C}_{ii}(q, \dot{q}) - \hat{C}_i(q_i, \dot{q}_i)]\dot{q}_i \right\}$$
$$+ [\bar{\hat{G}}_i(q) - \hat{G}_i(q_i)], \qquad (18)$$

where q_i, $\dot{q}_i$, $\ddot{q}_i$, $\bar{\hat{G}}_i(q)$, τ_{ic} and τ_{id} are the ith element of the vectors q, $\dot{q}$, $\ddot{q}$, $\hat{G}(q)$, τ_c and τ_d, respectively. $\hat{M}_{ij}(q)$, $\hat{C}_{ij}(q, \dot{q})$ are the ijth element of the matrices $\hat{M}(q)$, $\hat{C}(q, \dot{q})$, separately. Moreover, $\hat{M}_i(q_i)$, $\hat{C}_i(q_i, \dot{q}_i)$ and $\hat{G}_i(q_i, \dot{q}_i)$ represent the inertial term, Coriolis term and gravity term, respectively, which depend on local variables only. $Z_i(q, \dot{q}, \ddot{q})$ in Equation (18) represents all the coupling terms interconnected with other variables. It can been inferred from Equation (18) that the coupling terms of PM spherical actuator are very complex, which

should be compensated in the control law. The following properties of these terms can be revealed (Zhou, Li, & Shi, 2015).

Property 3.1: $\hat{M}_i(q_i)$ is symmetric, bounded and positive definite.

Property 3.2: $\dot{\hat{M}}_i(q_i) - 2\hat{C}_i(q_i, \dot{q}_i)$ is skew symmetric, i.e. for scalar functions $\hat{M}_i(q_i)$ and $\hat{C}_i(q_i, \dot{q}_i)$ in Equation (17), the following equation holds:

$$s_i{}^{\mathrm{T}}[\dot{\hat{M}}_i(q_i) - 2\hat{C}_i(q_i, \dot{q}_i)]s_i = 0, \quad \forall s_i \in \Re. \qquad (19)$$

Let

$$x_i = \begin{bmatrix} x_{i1} \\ x_{i2} \end{bmatrix} = \begin{bmatrix} q_i \\ \dot{q}_i \end{bmatrix}, \quad i = 1, 2, 3. \qquad (20)$$

Then each subsystem dynamics equation can be expressed by the following state equation:

$$S_i : \begin{cases} \dot{x}_{i1} = x_{i2}, \\ \dot{x}_{i2} = -p_i(q_i, \dot{q}_i, w_i) + \hat{M}_i^{-1}(q_i)\tau_{ic} + h_i(q, \dot{q}, \ddot{q}), \end{cases} \qquad (21)$$

where w_i is the same as τ_{id}, and x_i is the state vector of subsystem S_i, and:

$$p_i(q_i, \dot{q}_i, w_i) = \hat{M}_i^{-1}(q_i)[\hat{C}_i(q_i, \dot{q}_i)\dot{q}_i + \hat{G}_i(q_i) + \tau_{id}]$$
$$h_i(q, \dot{q}, \ddot{q}) = -\hat{M}_i^{-1}(q_i)Z_i(q, \dot{q}, \ddot{q}). \qquad (22)$$

Further, let

$$\theta_1 = [\dot{\alpha}, \alpha]$$
$$\theta_2 = [\dot{\beta}, \beta]$$
$$\theta_3 = [\dot{\gamma}, \gamma]$$
$$w = [w_\alpha, w_\beta, w_\gamma] = [w_1, w_2, w_3] = \tau_d$$
$$u = [u_{\tau_\alpha}, u_{\tau_\beta}, u_{\tau_\gamma}] = [u_{\tau_1}, u_{\tau_2}, u_{\tau_3}] = \tau_c. \qquad (23)$$

Equation (23) can be written as follows:

$$\begin{bmatrix} \ddot{\alpha} \\ \ddot{\beta} \\ \ddot{\gamma} \end{bmatrix} = - \begin{bmatrix} p_1(\theta_1, w_1) \\ p_2(\theta_2, w_2) \\ p_3(\theta_3, w_3) \end{bmatrix} + \begin{bmatrix} h_1(q, \dot{q}, \ddot{q}) \\ h_2(q, \dot{q}, \ddot{q}) \\ h_3(q, \dot{q}, \ddot{q}) \end{bmatrix}$$
$$+ \hat{M}(q)^{-1} \cdot \begin{bmatrix} u_{\tau_1} \\ u_{\tau_2} \\ u_{\tau_3} \end{bmatrix}. \qquad (24)$$

Herein, we define $p = [p_1, p_2, p_3]^{\mathrm{T}}$ as the subsystems of the dynamic model with uncertainties, while $h = [h_1, h_2, h_3]^{\mathrm{T}}$ is the dynamic couplings, since they are independent from the control law.

Then, introducing the virtual control input:

$$v = \hat{M}^{-1}(q) \cdot u = \begin{bmatrix} v_{\tau_1} \\ v_{\tau_2} \\ v_{\tau_3} \end{bmatrix}. \qquad (25)$$

Equation (23) can be further expressed as follows:

$$\begin{bmatrix} \ddot{\alpha} \\ \ddot{\beta} \\ \ddot{\gamma} \end{bmatrix} = -\begin{bmatrix} p_1(\theta_1, w_1) \\ p_2(\theta_2, w_2) \\ p_3(\theta_3, w_3) \end{bmatrix} + \begin{bmatrix} h_1(q, \dot{q}, \ddot{q}) \\ h_2(q, \dot{q}, \ddot{q}) \\ h_3(q, \dot{q}, \ddot{q}) \end{bmatrix} + \begin{bmatrix} v_{\tau_1} \\ v_{\tau_2} \\ v_{\tau_3} \end{bmatrix}. \qquad (26)$$

In this way, an AFSM algorithm controller can be designed for each subsystem in order to obtain the decentralised control in a multi-variable system.

3.2. Design of AFSM controller

Equation (24) can be considered as a set of coupled input/output equations with predetermined input/output pairings. The ith subsystem of dynamic model is:

$$\ddot{q}_i = -p_i(\theta_i, w_i) + h_i(q, \dot{q}, \ddot{q}) + v_{\tau_i}, \qquad (27)$$

where $i = 1,2,3$. To handle the above lumped disturbance of the PM spherical actuator system, an AFSM is designed for the trajectory tracking control. As this control scheme is based on the Lyapunov function, the stability of the closed-loop system can be ensured.

Let q^d be the desired trajectory, $x_{i1d} = q_i^d, x_{i2d} = \dot{q}_i^d$. The control strategy is described as follows.

The state tracking error of the motion is defined as:

$$e_{i1} = x_{i1} - x_{i1d},$$
$$e_{i2} = x_{i2} - x_{i2d}. \qquad (28)$$

Introduce the terminal sliding mode for the second order of the subsystem as:

$$s_i = \lambda_i e_{i1} + e_{i2} = x_{i2} - v_i, \qquad (29)$$

where λ_i is a positive constant, and v_i is the virtual controller which is chosen as:

$$v_i = \dot{x}_{i1d} - \lambda_i e_{i1}. \qquad (30)$$

Differentiating Equation (29) with respect to time yields

$$\dot{s}_i = \dot{e}_{i2} + \lambda_i \dot{e}_{i1} = -p_i + h_i + v_{\tau_i} - \dot{v}_i$$
$$= -\hat{M}_i^{-1} f_i - \hat{M}_i^{-1} \hat{C}_i s_i + h_i + v_{\tau_i}, \qquad (31)$$

where $f_i = f_i(\theta_i, w_i) = \hat{M}_i(p_i + \dot{v}_i) - \hat{C}_i s_i$. According to Equation (31), fuzzy logic systems are used to approximate the subsystems of dynamic model. An adaptive sliding mode controller is introduced to compensate for the effect of coupling term and fuzzy approximation error.

In order to estimate the nonlinear functions f_i, Takagi–Sugeno fuzzy model is used. The fuzzy IF-THEN rules are employed to perform a mapping from an input vector $x = [x_1, x_2, \ldots, x_n]^T \in \Re^n$ to an output $y \in \Re$. The lth fuzzy rule can be obtained from a collection of fuzzy IF-THEN rules in the following form (Chen et al., 2012):

$$R^l : \text{if } x_1 \text{ is } F_1^l(x_1), \ x_2 \text{ is } F_2^l(x_2), \cdots, \text{ and } x_n \text{ is } F_n^l(x_n),$$
$$\text{then } y_l = a_{l,0} + a_{l,1}x_1 + \cdots + a_{l,n}x_n, l = 1, 2, \ldots, k, \qquad (32)$$

where k is the number of fuzzy IF-THEN rules, F_j^l are fuzzy sets with memberships $\mu_{F_j^l}$, and y_l is a linguistic variable. By using singleton fuzzifier, product inference rule and centre-average defuzzifier, the output of the fuzzy logic system can be expressed as follows:

$$y = \frac{\sum_{l=1}^k y_l \left(\prod_{j=1}^n \mu_{F_j^l}(x_j) \right)}{\sum_{l=1}^k \left(\prod_{j=1}^n \mu_{F_j^l}(x_j) \right)} = \vartheta^T \psi(x), \qquad (33)$$

where $\vartheta = [a_{1,0}, \ldots, a_{k,0}, a_{1,1}, \ldots, a_{k,1}, \ldots, a_{1,n}, \ldots, a_{k,n}]^T$ is an adjustable parameter vector and $\psi = [\psi^1, \psi^2, \ldots, \psi^k]^T$ is a fuzzy function vector which is expressed as:

$$\psi^l(x) = \frac{\left(\prod_{j=1}^n \mu_{F_j^l}(x_j) \right)}{\sum_{l=1}^k \left(\prod_{j=1}^n \mu_{F_j^l}(x_j) \right)}. \qquad (34)$$

Based on the universal approximation theorem, $f_i(\theta_i, w_i)$ can be expressed as follows:

$$f_i(\theta_i, w_i) = \vartheta_i^T \psi_i(\theta_i, w_i) + \varepsilon_i, \qquad (35)$$

where ε_i is the approximation error of the fuzzy logic system and ϑ_i is the optimal parameter vector which satisfies:

$$\vartheta_i = \arg\min_{\hat{\vartheta}_i} \left\{ \sup_{\theta_i, w_i \in U_i} | f_i(\theta_i, w_i) - \hat{f}_i(\theta_i, w_i | \hat{\vartheta}_i) | \right\}, \qquad (36)$$

where U_i denotes the set of suitable bounds on θ_i and w_i, $\hat{\vartheta}_i$ is the adjustable parameter vector. $\hat{f}_i(\theta_i, w_i | \hat{\vartheta}_i)$ is an estimation of $f_i(\theta_i, w_i)$, which can be defined as:

$$\hat{f}_i(\theta_i, w_i | \hat{\vartheta}_i) = \hat{\vartheta}_i^T \psi_i(\theta_i, w_i). \qquad (37)$$

Assumption 3.1: The minimum estimation errors ε_i which is defined as:

$$\varepsilon_i = f_i(\theta_i, w_i) - \hat{f}_i(\theta_i, w_i | \hat{\vartheta}_i) \qquad (38)$$

is bounded, i.e. for all $\forall \theta_i, w_i \in U_i$, the following equation holds,

$$| \varepsilon_i | \le \xi_i \qquad (39)$$

that ξ_i is a positive constant.

Assumption 3.2: The coupling terms $Z_i(q, \dot{q}, \ddot{q})$ is bounded by:

$$| Z_i(q, \dot{q}, \ddot{q}) | \leq \sum_{j=1}^{N} d_{ij}S_j \leq \max_{ij}\{d_{ij}\} \sum_{j=1}^{N} S_j = \frac{\zeta_i}{N} \sum_{j=1}^{N} S_j,$$

(40)

where $d_{ij} \geq 0$, $S_j = 1 + | s_j | + | s_j |^2$ and $\zeta_i = N \max_{ij}\{d_{ij}\}$.

By virtue of Equation (27), the AFSM controller is now designed as:

$$u_{\tau_i} = \hat{\vartheta}_i \psi_i(\theta_i, w_i) - \hat{\xi}_i \text{sgn}(s_i) - \hat{\zeta}_i \text{sgn}(s_i)S_i - K_i s_i,$$

(41)

where K_i is a positive constant, and $\hat{\vartheta}_i$, $\hat{\xi}_i$, $\hat{\zeta}_i$ are estimations of ϑ_i, ξ_i, ζ_i, respectively. The estimation errors can be defined as:

$$\tilde{\vartheta}_i = \vartheta_i - \hat{\vartheta}_i,$$
$$\tilde{\xi}_i = \xi_i - \hat{\xi}_i,$$
$$\tilde{\zeta}_i = \zeta_i - \hat{\zeta}_i.$$

(42)

To generate control parameters in real time, adaptive laws to adjust the parameter vectors in Equation (41) need to be developed. The adaptive control rules are chosen as:

$$\dot{\hat{\vartheta}}_i = -\eta_i s_i \psi_i(\theta_i, w_i),$$
$$\dot{\hat{\xi}}_i = \sigma_i |s_i|,$$
$$\dot{\hat{\zeta}}_i = \varsigma_i |s_i| S_i,$$

(43)

where η_i, σ_i, ς_i are positive constants.

Above all, the subsystem of the dynamic model is assumed to be known as Equation (27), and the decentralised control law in Equation (41) is used to obtain reliable motion of the spherical actuator with possible configurations. Figure 5 shows the block diagram of the AFSM controller for each subsystem. The fuzzy controller represents the subsystem of dynamics expressed in terms of the sliding variables. The sliding mode controller is designed to handle the interconnections in system and compensate for errors of fuzzy approximation.

3.3. Convergence analysis

In this section, the convergence of proposed control scheme is analysed. Firstly, we choose the Lyapunov function as:

$$V = \sum_{i=1}^{3} \left[\frac{1}{2}\hat{M}_i s_i^T s_i + \frac{1}{2}\tilde{\vartheta}_i^T \eta_i^{-1} \tilde{\vartheta}_i \right. $$
$$\left. + \frac{1}{2}\tilde{\xi}_i^T \sigma_i^{-1} \tilde{\xi}_i + \frac{1}{2}\tilde{\zeta}_i^T \varsigma_i^{-1} \tilde{\zeta}_i \right].$$

(44)

Equation (42) yields:

$$\dot{\tilde{\vartheta}}_i = \dot{\vartheta}_i - \dot{\hat{\vartheta}}_i = -\dot{\hat{\vartheta}}_i,$$
$$\dot{\tilde{\xi}}_i = \dot{\xi}_i - \dot{\hat{\xi}}_i = -\dot{\hat{\xi}}_i,$$
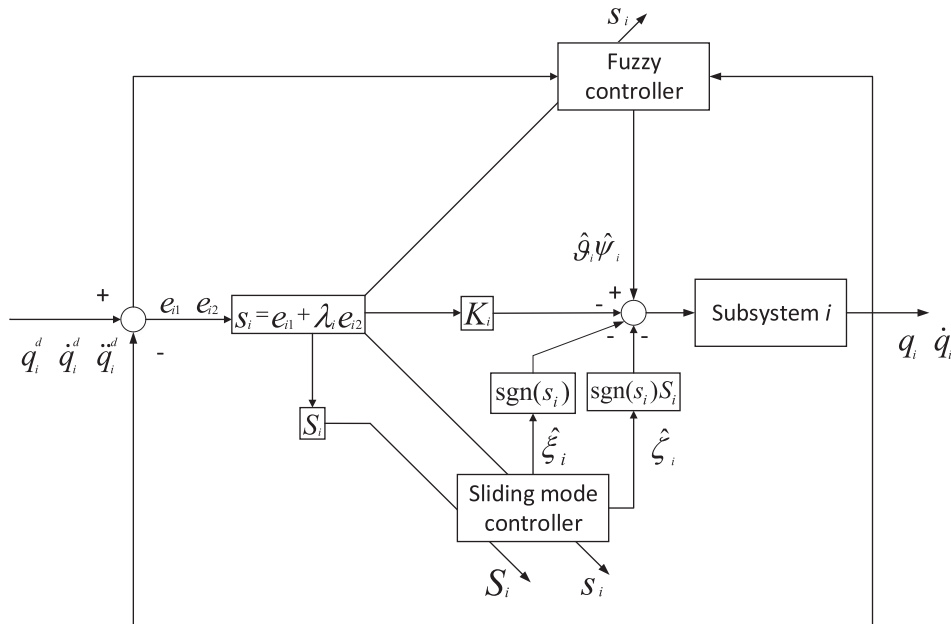$$\dot{\tilde{\zeta}}_i = \dot{\zeta}_i - \dot{\hat{\zeta}}_i = -\dot{\hat{\zeta}}_i.$$

(45)

Figure 5. Block diagram of the subsystem i.

Differentiating both sides of Equation (44) leads to

$$\dot{V} = \sum_{i=1}^{3}\left[\frac{1}{2}\dot{\hat{M}}_i s_i^T s_i + \hat{M}_i s_i^T \dot{s}_i - \tilde{\vartheta}_i^T \eta_i^{-1}\dot{\hat{\vartheta}}_i \right.$$
$$\left. - \tilde{\xi}_i^T \sigma_i^{-1}\dot{\hat{\xi}}_i - \tilde{\zeta}_i^T \varsigma_i^{-1}\dot{\hat{\zeta}}_i\right]. \tag{46}$$

Using Property 3.2 and Equations (31) and (46) becomes

$$\dot{V} = \sum_{i=1}^{3}\left[s_i^T\left(\frac{1}{2}\dot{\hat{M}}_i s_i + \hat{M}_i \dot{s}_i\right) - \tilde{\vartheta}_i^T \eta_i^{-1}\dot{\hat{\vartheta}}_i \right.$$
$$\left. - \tilde{\xi}_i^T \sigma_i^{-1}\dot{\hat{\xi}}_i - \tilde{\zeta}_i^T \varsigma_i^{-1}\dot{\hat{\zeta}}_i\right]$$

$$= \sum_{i=1}^{3}\left[s_i^T\left(\frac{1}{2}\dot{\hat{M}}_i s_i + \hat{M}_i(-\hat{M}_i^{-1}f_i(\theta_i, w_i) - \hat{M}_i^{-1}\hat{C}_i s_i\right.\right.$$
$$\left.\left. + h_i + v_{\tau_i})\right) - \tilde{\vartheta}_i^T \eta_i^{-1}\dot{\hat{\vartheta}}_i - \tilde{\xi}_i^T \sigma_i^{-1}\dot{\hat{\xi}}_i - \tilde{\zeta}_i^T \varsigma_i^{-1}\dot{\hat{\zeta}}_i\right]$$

$$= \sum_{i=1}^{3}\left[s_i^T(\frac{1}{2}\dot{\hat{M}}_i - \hat{C}_i)s_i + s_i^T\left(-f_i(\theta_i, w_i) + \hat{M}_i(h_i + v_{\tau_i})\right)\right.$$
$$\left. - \tilde{\vartheta}_i^T \eta_i^{-1}\dot{\hat{\vartheta}}_i - \tilde{\xi}_i^T \sigma_i^{-1}\dot{\hat{\xi}}_i - \tilde{\zeta}_i^T \varsigma_i^{-1}\dot{\hat{\zeta}}_i\right]$$

$$= \sum_{i=1}^{3}\left[s_i^T\left(-f_i(\theta_i, w_i) - Z_i(q, \dot{q}, \ddot{q}) + u_{\tau_i}\right)\right.$$
$$\left. - \tilde{\vartheta}_i^T \eta_i^{-1}\dot{\hat{\vartheta}}_i - \tilde{\xi}_i^T \sigma_i^{-1}\dot{\hat{\xi}}_i - \tilde{\zeta}_i^T \varsigma_i^{-1}\dot{\hat{\zeta}}_i\right]. \tag{47}$$

From Equation (35), one can obtain

$$\dot{V} = \sum_{i=1}^{3}\left[s_i^T\left(-f_i(\theta_i, w_i) - Z_i(q, \dot{q}, \ddot{q}) + u_{\tau_i}\right)\right.$$
$$\left. - \tilde{\vartheta}_i^T \eta_i^{-1}\dot{\hat{\vartheta}}_i - \tilde{\xi}_i^T \sigma_i^{-1}\dot{\hat{\xi}}_i - \tilde{\zeta}_i^T \varsigma_i^{-1}\dot{\hat{\zeta}}_i\right]$$

$$= \sum_{i=1}^{3}\left[s_i^T\left(-\vartheta_i^T\psi_i(\theta_i, w_i) - \varepsilon_i - Z_i(q, \dot{q}, \ddot{q}) + u_{\tau_i}\right)\right.$$
$$\left. - \tilde{\vartheta}_i^T \eta_i^{-1}\dot{\hat{\vartheta}}_i - \tilde{\xi}_i^T \sigma_i^{-1}\dot{\hat{\xi}}_i - \tilde{\zeta}_i^T \varsigma_i^{-1}\dot{\hat{\zeta}}_i\right]. \tag{48}$$

By substituting Equation (41) into (48) and using Equations (40) and (42), we have:

$$\dot{V} = \sum_{i=1}^{3}\left[s_i^T\left(-\vartheta_i^T\psi_i(\theta_i, w_i) - \varepsilon_i + \hat{\vartheta}_i\psi_i(\theta_i, w_i)\right.\right.$$
$$\left.\left. - \hat{\xi}_i\text{sgn}(s_i) - \hat{\zeta}_i\text{sgn}(s_i)S_i - K_i s_i - Z_i(q, \dot{q}, \ddot{q})\right)\right.$$
$$\left. - \tilde{\vartheta}_i^T \eta_i^{-1}\dot{\hat{\vartheta}}_i - \tilde{\xi}_i^T \sigma_i^{-1}\dot{\hat{\xi}}_i - \tilde{\zeta}_i^T \varsigma_i^{-1}\dot{\hat{\zeta}}_i\right]$$

$$\leq \sum_{i=1}^{3}\left[s_i^T\left(-\tilde{\vartheta}_i\psi_i(\theta_i, w_i) - \varepsilon_i - \hat{\xi}_i\text{sgn}(s_i)\right.\right.$$
$$\left.\left. - \hat{\zeta}_i\text{sgn}(s_i)S_i - K_i s_i\right) - \tilde{\vartheta}_i^T \eta_i^{-1}\dot{\hat{\vartheta}}_i\right.$$
$$\left. - \tilde{\xi}_i^T \sigma_i^{-1}\dot{\hat{\xi}}_i - \tilde{\zeta}_i^T \varsigma_i^{-1}\dot{\hat{\zeta}}_i\right] + \sum_{i=1}^{3}|s_i|\left|Z_i(q, \dot{q}, \ddot{q})\right|$$

$$\leq \sum_{i=1}^{3}\left[s_i^T\left(-\tilde{\vartheta}_i\psi_i(\theta_i, w_i) - \varepsilon_i - \hat{\xi}_i\text{sgn}(s_i)\right.\right.$$
$$\left.\left. - \hat{\zeta}_i\text{sgn}(s_i)S_i - K_i s_i\right) - \tilde{\vartheta}_i^T \eta_i^{-1}\dot{\hat{\vartheta}}_i\right.$$
$$\left. - \tilde{\xi}_i^T \sigma_i^{-1}\dot{\hat{\xi}}_i - \tilde{\zeta}_i^T \varsigma_i^{-1}\dot{\hat{\zeta}}_i\right] + \sum_{i=1}^{3}|s_i|\sum_{j=1}^{3}d_{ij}S_j. \tag{49}$$

Noticing that $|s_i| \leq |s_j| \Leftrightarrow S_i \leq S_j$, the following inequality is obtained from Chebyshev inequality

$$\sum_{i=1}^{N}|s_i|\sum_{j=1}^{N}S_j \leq N\sum_{i=1}^{N}|s_i| S_j. \tag{50}$$

With Equations (39), (40) and (50), Equation (49) becomes

$$\dot{V} \leq \sum_{i=1}^{3}\left[s_i^T\left(-\tilde{\vartheta}_i\psi_i(\theta_i, w_i) - \varepsilon_i - \hat{\xi}_i\text{sgn}(s_i)\right.\right.$$
$$\left.\left. - \hat{\zeta}_i\text{sgn}(s_i)S_i - K_i s_i\right) - \tilde{\vartheta}_i^T \eta_i^{-1}\dot{\hat{\vartheta}}_i\right.$$
$$\left. - \tilde{\xi}_i^T \sigma_i^{-1}\dot{\hat{\xi}}_i - \tilde{\zeta}_i^T \varsigma_i^{-1}\dot{\hat{\zeta}}_i\right] + \zeta_i\sum_{i=1}^{3}|s_i| S_i$$

$$\leq \sum_{i=1}^{3}\left[s_i^T\left(-\tilde{\vartheta}_i\psi_i(\theta_i, w_i) - K_i s_i\right) - \tilde{\vartheta}_i^T \eta_i^{-1}\dot{\hat{\vartheta}}_i\right.$$
$$\left. - \tilde{\xi}_i^T \sigma_i^{-1}\dot{\hat{\xi}}_i - \tilde{\zeta}_i^T \varsigma_i^{-1}\dot{\hat{\zeta}}_i + |\varepsilon_i||s_i|\right.$$
$$\left. - \hat{\xi}_i\text{sgn}(s_i)s_i - \hat{\zeta}_i\text{sgn}(s_i)s_iS_i + \zeta_i|s_i| S_i\right]$$

$$\leq \sum_{i=1}^{3}\left[s_i^T\left(-\tilde{\vartheta}_i\psi_i(\theta_i, w_i) - K_i s_i\right) - \tilde{\vartheta}_i^T \eta_i^{-1}\dot{\hat{\vartheta}}_i\right.$$
$$\left. - \tilde{\xi}_i^T \sigma_i^{-1}\dot{\hat{\xi}}_i - \tilde{\zeta}_i^T \varsigma_i^{-1}\dot{\hat{\zeta}}_i\right.$$
$$\left. + \tilde{\xi}_i|s_i| + \tilde{\zeta}_i|s_i| S_i\right]. \tag{51}$$

Substituting Equation (43) into (51) yields:

$$\dot{V} \leq \sum_{i=1}^{3}-s_i^T K_i s_i. \tag{52}$$

Then Equation (52) can satisfy:

$$\dot{V} \leq 0. \tag{53}$$

As a result, the global stability of the proposed control algorithm is guaranteed and the tracking errors converge to zero.

4. Simulations

Simulations have been carried out using different control strategies. One simulation was performed with varying modelling errors with a fixed load torque and varying different loads with a fixed coefficient of the modelling errors. In another simulation, the nutation motion was adopted to verify the global controllability of the proposed algorithm. The trajectory tracking performances with different controllers are analysed and compared.

The modelling errors are set as:

$$\Delta M(q) = m \cdot M(q), \Delta C(q, \dot{q}) = m \cdot C(q, \dot{q}), \Delta G(q, \dot{q})$$
$$= [0.002, 0.001, 0.001], \tag{54}$$

where m is the coefficient quantifying the modelling error.

The random external disturbance torque is set as:

$$\tau_d = \tau_l + \tau_r, \tag{55}$$

where the load torque and the random external disturbance torque are set as:

$$\tau_r = r \cdot [\cos(\pi t) \quad \sin(-\pi t) \quad \exp(\pi t)]$$
$$\tau_l = L \cdot [0.05 \quad 0.05 \quad 0.05], \tag{56}$$

where L denotes the coefficient of the load torque. r is the coefficient of the random external disturbance torque and randomly distributed in $(-0.05 \ 0.05)$.

The fuzzy sets of a FLS with Gaussian Function for each input signal are divided as {NB, NS, ZO, PS, PB}. Meanwhile, the membership functions are chosen as:

$$\mu_{F_j^l}(x_j) = exp\left[-b\left(\frac{x_j - c}{2\sigma}\right)^2\right], \tag{57}$$

where $b = \frac{1}{2}, c \in \{-3, -1.5, 0, 1.5, 3\}$ and $\sigma = 1$.
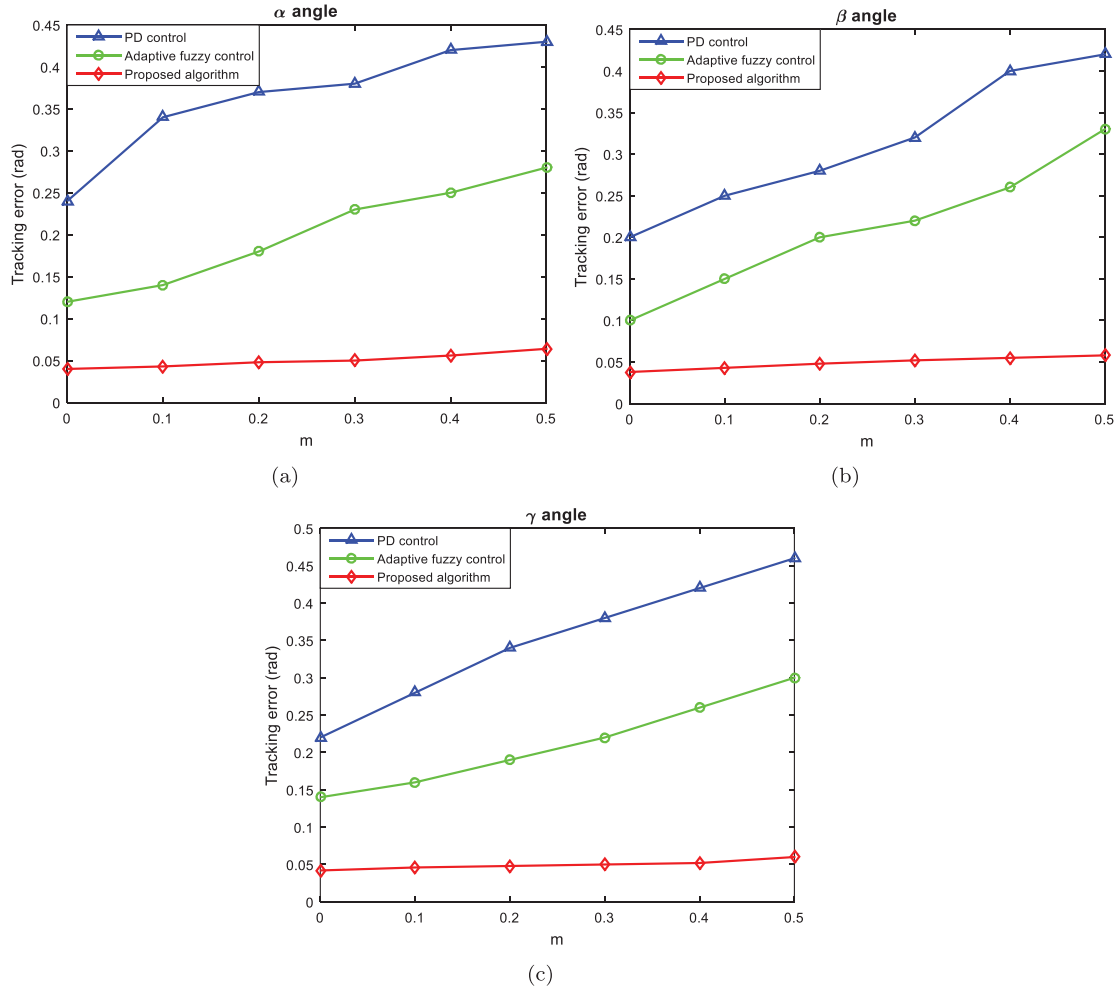

Figure 6. Comparison of sinusoidal trajectory tracking errors with different algorithms ($L = 1$ with varying m).

To ensure the convergence and robustness of the proposed control scheme, the controller gain matrices are set as:

$$K = \text{diag}[20 \quad 20 \quad 20],$$
$$\lambda = \text{diag}[50 \quad 50 \quad 50]. \tag{58}$$

The parameters of the adaptive controller are set as $\vartheta = 10, \xi = 10$ and $\zeta = 10$. It is noted that the parameters of the compared adaptive fuzzy logic controller are equal to those of the proposed controller.

4.1. Sinusoidal trajectory tracking in different conditions

In the first simulation, sinusoidal trajectory tracking for three channels were conducted in different conditions. In addition, the static and dynamic performances of proposed algorithm are compared with different control methods. Herein, we firstly set the coefficient of the load torque L as 1 ($L=1$) and change the coefficient of the modelling error m from 0 to 0.5. Afterwards, we set the

coefficient of the modelling error m as 0.2 ($m=0.2$) and change the coefficient of the load torque L from 0 to 5.

Figure 6 shows the sinusoidal trajectory tracking errors with variation of the coefficient of the modelling error m from 0 to 0.5. It is seen that the tracking errors of the proposed control is the smallest among three control methods during the change of m. When PD and adaptive fuzzy logic control scheme are applied with the condition $m=0.2$, the maximum position tracking errors of three Euler angles α, β, and γ are 0.4376, 0.4121, 0.4687 (rad) and 0.2505, 0.2822, 0.2669 (rad), respectively. In comparison, under the proposed method, the corresponding position errors are reduced to 0.0832, 0.0750 and 0.0761 (rad). Figure 7 shows the sinusoidal trajectory tracking errors when the coefficient of the load torque L varies from 0 to 5. It is clear that the tracking errors of the proposed control are much smaller than those of other two control methods as L changes. Under the condition $L=2$, the maximum position tracking errors of three Euler angles α, β, and γ are 1.2560, 1.0560, 1.1500 (rad) and 0.8954, 0.9856, 1.0100 (rad) by PD and adaptive fuzzy
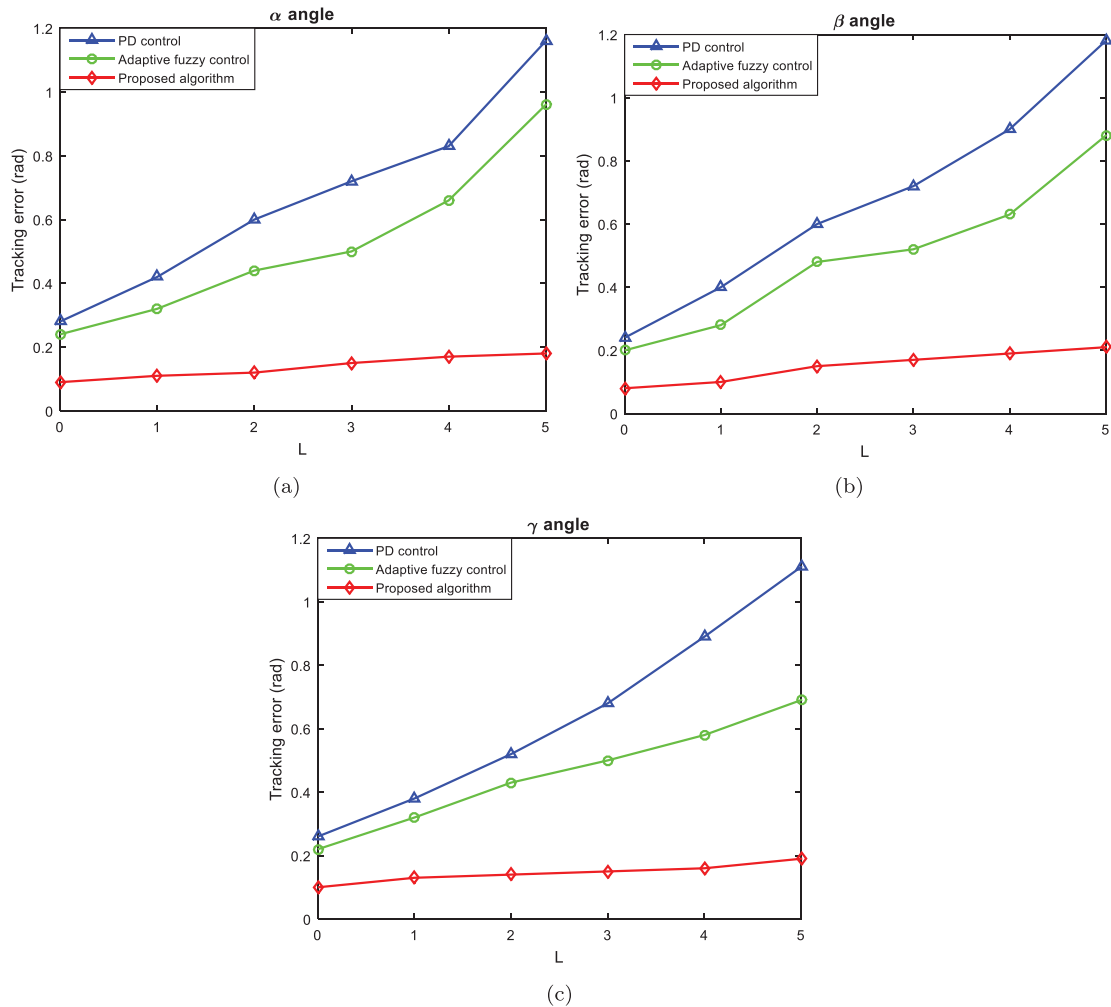

Figure 7. Comparison of sinusoidal trajectory tracking errors of different algorithms ($m=0.2$ with varying L).

controls, respectively. On the other hand, with the proposed control, the corresponding Euclidean norms are 0.1854, 0.1986 and 0.1769 (rad).

These results indicate that the proposed control algorithm can greatly improve the tracking performance in the presence of different conditions, demonstrating the effectiveness and robustness of the proposed algorithm.

4.2. Nutation motion

The nutation motion is a gyro-movement, which can make a good observation of global controllability. The system uncertainties are set as $L = 2$ and $m = 0.2$. The desired trajectory is:

$$q(t) = \begin{bmatrix} \alpha \\ \beta \\ \gamma \end{bmatrix} = \begin{bmatrix} 0.2\sin(\pi t) \\ 0.2t\cos(\pi t) \\ 2\pi t \end{bmatrix}, t \in [0, 5]. \quad (59)$$

The tracking performances of the PM spherical actuator with different control algorithm are shown in Figure 8, where q denotes the actual output, and qd is the desired trajectory. It can be clearly seen from Figure 8(a) that there is an obvious tracking error in PD control strategy,

which means that interaction among inter-axis and uncertainties with different loads and modelling errors seriously affect the nutation motion tracking performance. Figure 8(b ,c) show that the proposed algorithm can track the desired trajectory precisely in comparison to adaptive fuzzy control strategy, which indicates that proposed algorithm can greatly improve the static and dynamic responses of nutation motion by eliminating the effect of inter-axis couplings. It also means that the algorithm proposed in this paper has relatively good global controllability in the presence of uncertainties with different loads and modelling errors.

5. Experiments

Further to the simulations, experiments were conducted with a prototype of the PM spherical actuator. The control system is shown in Figure 9. The system includes a graphical user interface for parameter settings, a PC in charge of algorithm computation. With the system, the commands are sent to the current controller which is constructed by ARM and FPGA, and the power of output currents is amplified by FPGA. In the experiments, the

(a) Tracking performance with the PD control.

(b) Tracking performance with the adaptive fuzzy control.

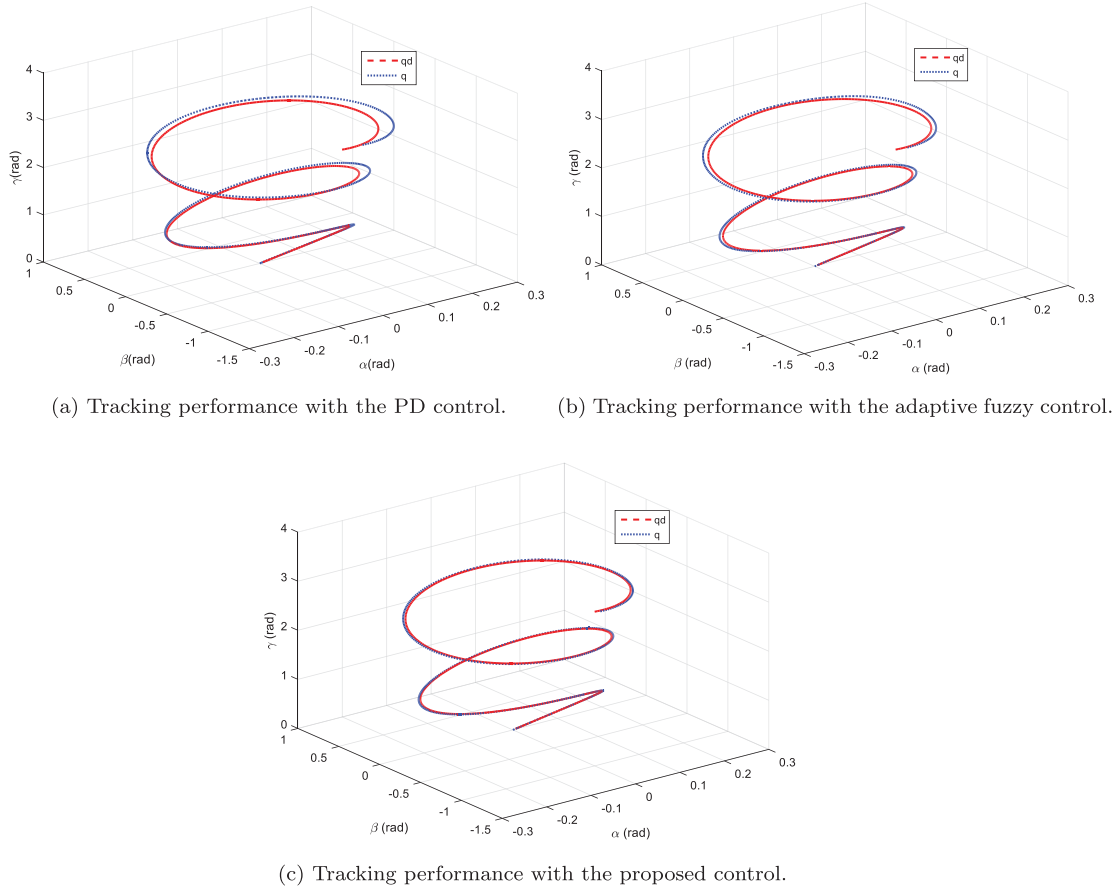(c) Tracking performance with the proposed control.

Figure 8. Comparison of tracking performance in nutation motion. (a) Tracking performance with the PD control. (b) Tracking performance with the adaptive fuzzy control. (c) Tracking performance with the proposed control.
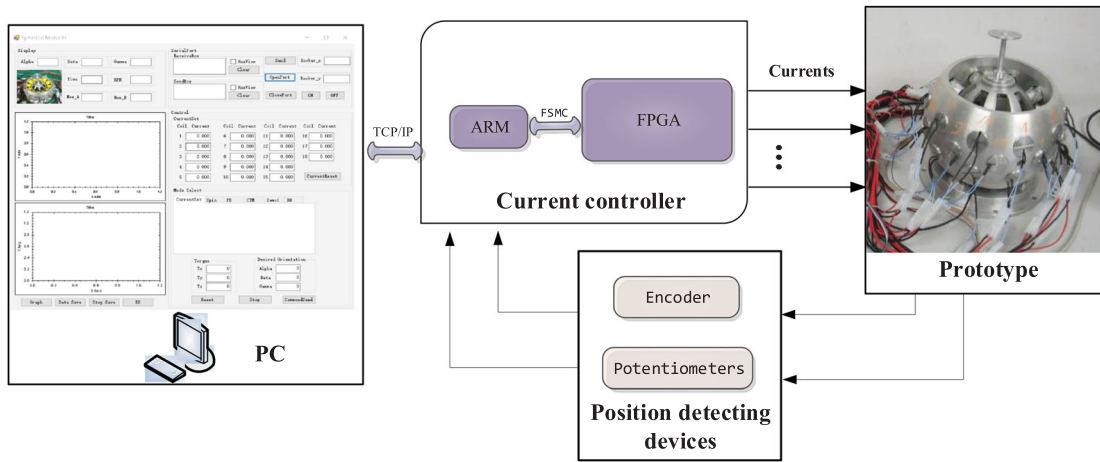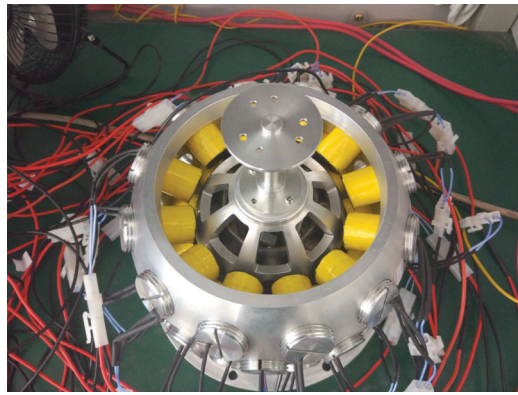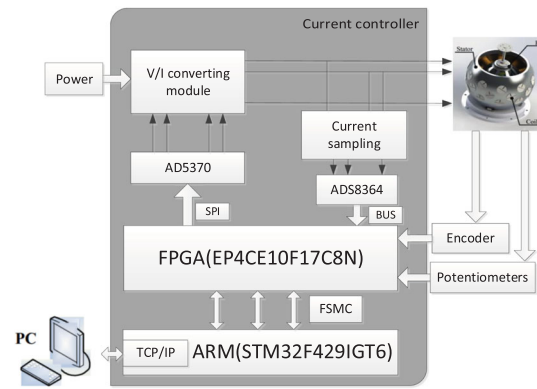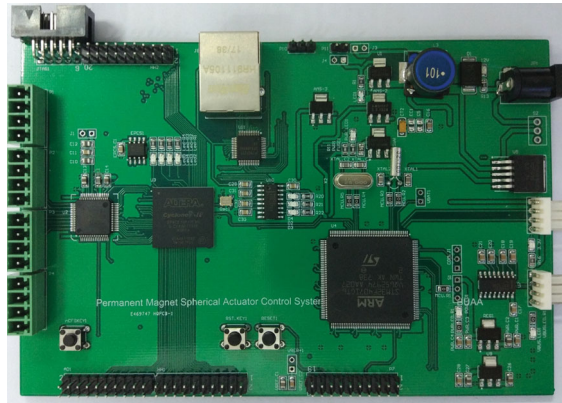
Figure 9. General diagram of PM spherical actuator's control system.

(a) Experimental prototype.

(b) Block diagram of the control system.

(c) Core control module.

Figure 10. Experimental prototype and the control system. (a) Experimental prototype. (b) Block diagram of the control system. (c) Core control module.

3-DOF motions were measured by position detecting device. The hardwares of the PM spherical actuator are shown in Figure 10(a) with block diagram of the current control system shown in Figure 10(b). As shown in Figure 10, the ARM and FPGA comprise the core control module. The ARM is responsible for communicating with the PC and algorithm computing. FPGA is in charge of driving the AD5370 chip and processing sensors information. The D/A chip AD5370 has 40 channels with 16-bit D/A converting resolution for generating multi-channel and bipolar currents simultaneously. The V-I converting circuit OPA549 (a power amplifier) is

chosen to achieve V/I conversion, which can transform the voltage obtained from AD5370 into a proportional current. The ADS8364 is an A/D chip that can offer 6-channel output with a 16-bit A/D converting resolution. Orientation module system includes an rotary encoder OME-500-2MCA and a two-axis potentiometer sensor RV24YN20S which provide high precision position measurement. A graphical user interface (GUI) program is developed on the PC in VS2016 environment programmed by C++. Hence, the control parameter setting, control mode selection, command sending and status displaying can be easily done through GUI.

To observe the control performance simply, a typical tilting motion along the X-axis of rotor is conducted. In this experiment, a load weighting, 0.05 kg, is fixed on the output shaft. The rotor is controlled to move along the desired trajectory $q(t) = [\alpha(t), 0, 0], t \in [0, 6]$ with:

$$
\alpha(t) =
\begin{cases}
\dfrac{\pi}{30}t, & 0 \leq t \leq 2, \\[2mm]
\dfrac{\pi}{15}, & 2 \leq t \leq 4, \\[2mm]
-\dfrac{\pi}{30}t + \dfrac{\pi}{5}, & 4 \leq t \leq 6.
\end{cases}
\tag{60}
$$
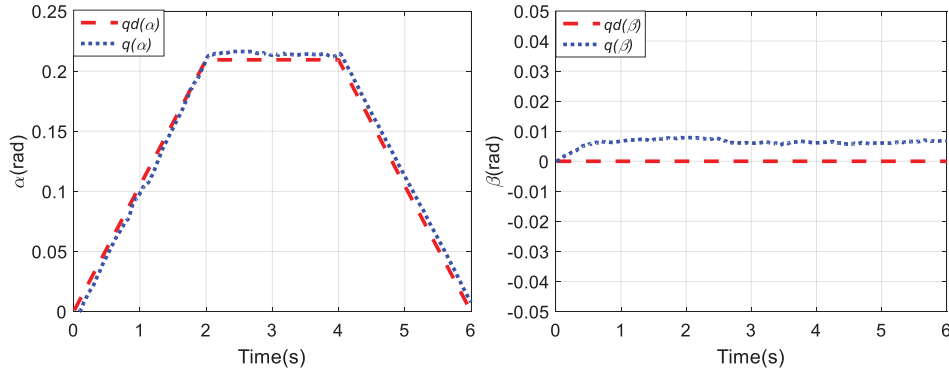
(a) Tracking performance under the PD control.
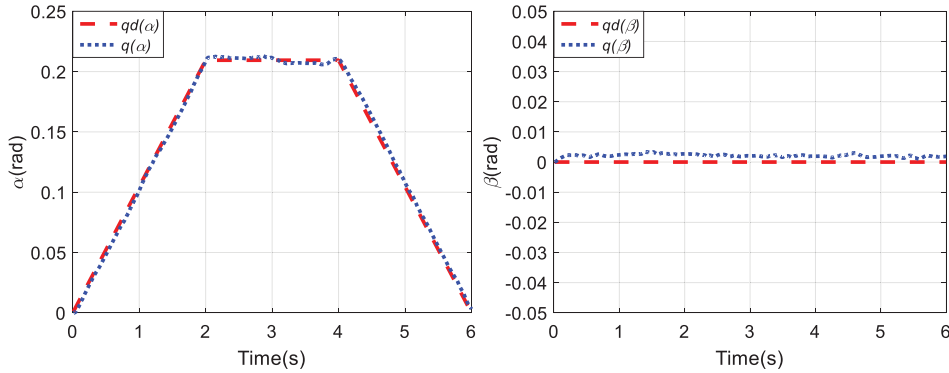
(b) Tracking performance under the adaptive fuzzy control.
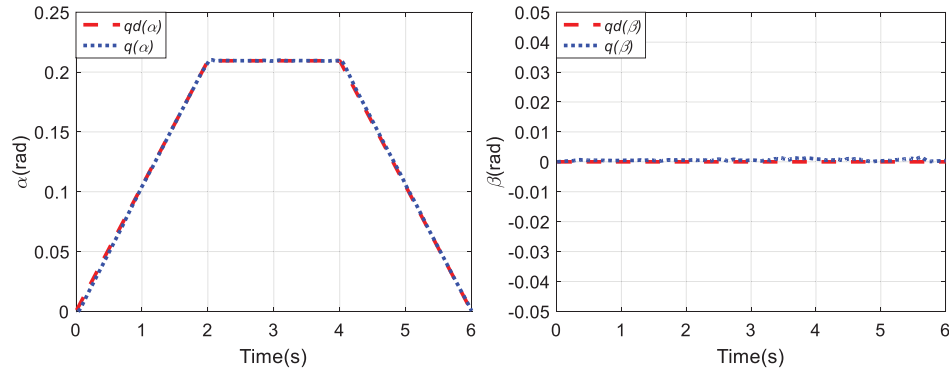
(c) Tracking performance under the proposed control.

Figure 11. Experimental results of tracking performance under different methods. (a) Tracking performance under the PD control. (b) Tracking performance under the adaptive fuzzy control. (c) Tracking performance under the proposed control.

Herein, a comparison is made about the trajectory tracking control performance among the classical PD control, the conventional adaptive fuzzy control and the proposed control. Figure 11(a) shows the trajectory tracking performance under the classical PD control. It is obvious that the maximum tracking errors of both α and β angles are more than 0.55°. The undesirable dynamic response indicates that the classical PD control is not applicable for PM spherical actuator in the presence of nonlinearities and uncertainties as well as inter-axis couplings. Figure 11(b) shows the experimental results under conventional adaptive fuzzy control strategy. It can be seen that the actual trajectory has a better tracking performance than PD control, and the maximum tracking error reduces to about 0.25°. The results indicate that the complicated uncertainties in the practical control system have been eliminated effectively. However, it can be observed that there exists an unacceptable deviation around the initial value, although the given trajectory of Y-axis is 0. It should be attributed to the inter-axis coupling influences from X-axis.

It is seen from Figure 11(c) that the actual trajectory fits the desired trajectory well under the proposed control scheme. The tracking errors are clearly smaller than those of above control strategies, and the maximum tracking error is only about 0.12°. The experimental results illustrate that our proposed algorithm is robust against complex internal and external uncertainties, which can also compensate for the effect of inter-axis couplings of α and β accurately.

In summary, the experimental results show that the proposed control algorithm can give much better trajectory tracking performances in practical systems, compared to the PD control and conventional adaptive fuzzy control. Furthermore, the fuzzy approximate terms can make the system robust against various kind of uncertainties including modelling errors and external disturbances, while inter-axis coupling influences have been successfully compensated by the sliding mode term. The adaptive law with self-adaptive ability can improve the robustness of the control system.

6. Conclusions

This paper investigates the trajectory tracking control of the PM spherical actuator. The nonlinear dynamic model of the PM spherical actuator with uncertainties and strong inter-axis couplings was established based on the Lagrange equation. To cope with the uncertainties and couplings of PM spherical actuators, an AFSM-based decentralised control was developed. The stability analysis of the control system is performed by Lyapunov function and the performance of the algorithm is tested by both simulations and experiments.

A major contribution of this paper is the introduction of AFSM-based decentralised control to PM spherical actuator. The proposed algorithm is a hybrid control scheme, combining the merits of decentralised control, fuzzy logic systems and sliding mode control. The decentralised control can eliminate the inter-axis couplings among the input/output pairs by partitioning the MIMO system into three separate SISO subsystems. The fuzzy logic systems are applied to approximate each subsystem with lumped uncertainties that are caused by modelling errors, random influence and the load error. The effect of coupling terms and fuzzy approximation error are compensated by introducing the adaptive sliding mode law. Simulation and experimental results verify the proposed algorithm and its better performance over conventional PD and adaptive fuzzy control methods.

Furthermore, the tracking errors of the proposed algorithm increase with the increasing load torque from the simulation results. In the future, the algorithm can be improved to adapt the varying load torques with better trajectory performance.

Acknowledgements

Disclosure statement

Funding

Notes on contributors

Jingmeng Liu received the B.S. degree from Anhui Polytechnic University, Wuhu, China, in 1991 and the M.S. and Ph.D. degrees from Beihang University, Beijing, China, in 2000 and 2004, respectively. He is currently an Associate Professor with the School of Automation Science and Electrical Engineering, Beihang University. His current research interests include actuators, precision control, and mechatronics.

Xuerong Li received the B.S. degree from China Agricultural University, China, in 2012. She is currently working towards the Ph.D. degree in School of Automation Science and Electrical Engineering, Beihang University, China. Her current research interests include parallel robots, actuators and control systems.

Shaoxiong Cai received the B.S. degree from Beijing Jiaotong University, Beijing, China, in 2009. He is currently working toward the M.S. degree in the School of Automation Science

and Electrical Engineering, Beihang University, Beijing, China. His current research interests include robots, control, and navigation systems.

Weihai Chen received the B.S. degree from Zhejiang University, Hangzhou, China, in 1982 and the M.S. and Ph.D. degrees from Beihang University, Beijing, China, in 1988 and 1996, respectively. He is currently a Professor with the School of Automation Science and Electrical Engineering, Beihang University. His current research interests include modular robots, actuators, automation, and control.

Shaoping Bai received the Ph.D. Degree in Mechanical and Production Engineering from the Nanyang Technological University, Singapore in 2001, the M.Eng. Degree from Tsinghua University and B.S. Degree from Harbin Institute of Technology in 1993 and 1988, respectively. He is currently an Associate Professor at the Department of Materials and Production, Aalborg University (AAU), Denmark. His research interests include dynamics and design, medical and assistive robots, parallel manipulators, and walking robots. He is a member of ASME and IEEE Robotics and Automation.

References

Bai, S., Hansen, M. R., & Andersen, T. O. (2009). Modelling of a special class of spherical parallel manipulators with Euler parameters. *Robotica*, *27*(2), 161–170. doi:10.1017/S0263574708004402

Bai, K., & Lee, K. M. (2014). Direct field-feedback control of a ball-joint-like permanent-magnet spherical motor. *IEEE/ASME Transactions on Mechatronics*, *19*(3), 975–986. doi:10.1109/TMECH.2013.2264565

Bartolini, G., Levant, A., Pisano, A., & Usai, E. (2016). Adaptive second-order sliding mode control with uncertainty compensation. *International Journal of Control*, *89*(9), 1747–1758. doi:10.1080/00207179.2016.1142616

Chen, B., Lin, C., Liu, X., & Liu, K. (2016). Observer-based adaptive fuzzy control for a class of nonlinear delayed systems. *IEEE Transactions on Systems Man & Cybernetics Systems*, *46*(1), 27–36. doi:10.1109/TSMC.2015.2420543

Chen, B., Liu, X. P., Ge, S. S., & Lin, C. (2012). Adaptive fuzzy control of a class of nonlinear systems by fuzzy approximation approach. *IEEE Transactions on Fuzzy Systems*, *20*(6), 1012–1021. doi:10.1109/TFUZZ.2012.2190048

Chen, W., Zhang, L., Yan, L., & Liu, J. (2012). Design and control of a three degree-of-freedom permanent magnet spherical actuator. *Sensors & Actuators A Physical*, *180*, 75–86. doi:10.1016/j.sna.2012.04.010

Chu, J., Niguchi, N., & Hirata, K. (2013). Feedback control of outer rotor spherical actuator using adaptive neuro-fuzzy inference system. *International conference on sensing technology*, Wellington, New Zealand, (pp. 401–405).

Dehez, B., Grenier, D., & Raucent, B. (2002). Two-degree-of-freedom spherical actuator for Omnimobile Robot. *International conference on robotics and Automation*, Washington, DC (pp. 2381–2386).

Fang, Y., Fei, J., & Hu, T. (2018). Adaptive backstepping fuzzy sliding mode vibration control of flexible structure. *Journal of Low Frequency Noise, Vibration and Active Control*, 1–18. doi:10.1177/1461348418767097

Fei, J., & Lu, C. (2018). Adaptive fractional order sliding mode controller with neural estimator. *Journal of the Franklin Institute*, *355*(5), 2369–2391. doi:10.1016/j.jfranklin.2018.01.006

Feng, G. (2006). A survey on analysis and design of model-based fuzzy control systems. *IEEE Transactions on Fuzzy Systems*, *14*(5), 676–697. doi:10.1109/TFUZZ.2006.883415

Hey, J., Teo, T. J., Bui, V. P., Yang, G., & Martinez-Botas, R. (2014). Electromagnetic actuator design analysis using a two-stage optimization method with coarse-fine model output space mapping. *IEEE Transactions on Industrial Electronics*, *61*(10), 5453–5464. doi:10.1109/TIE.2014.2301727

Jia, Y. (2000). Robust control with decoupling performance for steering and traction of 4WS vehicles under velocity-varying motion. *IEEE Transactions on Control Systems Technology*, *8*(3), 554–569. doi:10.1109/87.845885

Jia, Y. (2003). Alternative proofs for improved LMI representations for the analysis and the design of continuous-time systems with polytopic type uncertainty: A predictive approach. *IEEE Transactions on Automatic Control*, *48*(8), 1413–1416. doi:10.1109/TAC.2003.815033

Li, X., Liu, J., Chen, W., & Bai, S. (2018). Integrated design, modeling and analysis of a novel spherical motion generator driven by electromagnetic principle. *Robotics and Autonomous Systems*, *106*, 69–81. doi:10.1016/j.robot.2018.04.006

Lim, C. K., Chen, I. M., Yan, L., Yang, G., & Lee, K. M. (2009). Electromechanical modeling of a permanent-magnet spherical actuator based on magnetic-dipole-moment principle. *IEEE Transactions on Industrial Electronics*, *56*(5), 1640–1648. doi:10.1109/TIE.2008.2009526

Liu, J., Deng, H., Chen, W., & Bai, S. (2017). Robust dynamic decoupling control for permanent magnet spherical actuators based on extended state observer. *IET Control Theory & Applications*, *11*(5), 619–631. doi:10.1049/iet-cta.2016.0551

Liu, J., Deng, H., Hu, C., Hua, Z., & Chen, W. (2017). Adaptive backstepping sliding mode control for 3-DOF permanent magnet spherical actuator. *Aerospace Science & Technology*, *67*, 62–71. doi:10.1016/j.ast.2017.03.032

Ma, Y., Na, Z., & Zhong, X. (2013). Decentralized robust control for uncertain nonlinear descriptor large-scale composite systems with input saturation. *International Journal of Innovative Computing Information & Control*, *9*(10), 3991–4000.

Maeda, S., Hirata, K., Ikejiri, S., & Tong, M. (2010). Feedback control of electromagnetic spherical actuator with three-degree-of-freedom. In *XIX international conference on electrical machines*, Rome, Italy, (pp. 1–6).

Murray, R. M., Sastry, S. S., & Li, Z. (1994). *A mathematical introduction to robotic manipulation*. Boca Raton, FL: CRC Press, Inc.

Shen, Q., Shi, P., & Shi, Y. (2016). Distributed adaptive fuzzy control for nonlinear multiagent systems via sliding mode observers. *IEEE Transactions on Cybernetics*, *46*(12), 3086–3097. doi:10.1109/TCYB.2015.2496963

Shigeki, T., Shigeru, S., Zhang, G., Yasutaro, M., & Kazuto, N. (1995). Multi degree of freedom spherical ultrasonic motor. *International conference on robotics and automation*, Nagoya, Japan, (Vol. 3, pp. 2935–2940).

Son, H., & Lee, K. M. (2010). Open-loop controller design and dynamic characteristics of a spherical wheel motor. *IEEE Transactions on Industrial Electronics*, *57*(10), 3475–3482. doi:10.1109/TIE.2009.2039454

Son, H., & Lee, K. M. (2014). Control system design and input shape for orientation of spherical wheel motor. *Control Engineering Practice*, 24, 120–128. doi:10.1016/j.conengprac.2013.11.013

Takahara, K., Hirata, K., Niguchi, N., Nishiura, Y., & Sakaidani, Y. (2017). Experimental evaluation of the static characteristics of multi-degree-of-freedom spherical actuators. *IEEE Transactions on Magnetics*, 53(11), 1–5. doi:10.1109/TMAG.2017.2717870

Tang, Y., Tomizuka, M., Guerrero, G., & Montemayor, G. (2000). Decentralized robust control of mechanical systems. *IEEE Transactions on Automatic Control*, 45(4), 771–776. doi:10.1109/9.847120

Toyama, S., & Kobayashi, A. (1996). Development of spherical ultrasonic motor. *CIRP Annals-Manufacturing Technology*, 45(1), 27–30. doi:10.1016/S0007-8506(07)63010-8

Utkin, V., Guldner, J., & Shi, J. (2009). *Sliding mode control in electro-mechanical systems*. Boca Raton, FL: CRC Press.

Wang, C., & Lin, Y. (2015). Decentralized adaptive tracking control for a class of interconnected nonlinear time-varying systems. *Automatica*, 54, 16–24. doi:10.1016/j.automatica.2015.01.041

Wang, H., Liu, W., Qiu, J., & Liu, P. X. (2017). Adaptive fuzzy decentralized control for a class of strong interconnected nonlinear systems with unmodeled dynamics. *IEEE Transactions on Fuzzy Systems*, 26(2), 836–846. doi:10.1109/TFUZZ.2017.2694799

Wang, W., Wang, J., Jewell, G. W., & Howe, D. (2003). Design and control of a novel spherical permanent magnet actuator with three degrees of freedom. *IEEE/ASME Transactions on Mechatronics*, 8(4), 457–468. doi:10.1109/TMECH.2003.820003

Xia, C., Song, P., Li, H., Li, B., & Shi, T. (2009). Research on torque calculation method of permanent-magnet spherical motor based on the finite-element method. *IEEE Transactions on Magnetics*, 45(4), 2015–2022. doi:10.1109/TMAG.2009.2012390

Yan, L., Chen, I. M., Lim, C. K., Yang, G., & Lee, K. M. (2011). *Design, modeling and experiments of 3-DOF electromagnetic spherical actuators*. Dordrecht: Springer.

Yan, L., Zhang, L., Zhu, B., Zhang, J., & Jiao, Z. (2017). Single neural adaptive controller and neural network identifier based on PSO algorithm for spherical actuators with 3D magnet array. *Review of Scientific Instruments*, 88(10), 105001. doi:10.1063/1.5004677

Zhang, L., Chen, W., Yan, L., & Liu, J. (2011). Trajectory planning and current control optimization of three degree-of-freedom spherical actuator. *IEEE/RSJ international conference on intelligent robots and systems*, San Francisco, CA, USA (pp. 744–749).

Zheng, W., Wu, G., Xu, G., & Chen, X. (2015). Adaptive fuzzy sliding-mode control of uncertain nonlinear system. *International conference on management, education, information and control*, Shenyang, China (pp. 707–711).

Zhou, Q., Li, H., & Shi, P. (2015). Decentralized adaptive fuzzy tracking control for robot finger dynamics. *IEEE Transactions on Fuzzy Systems*, 23(3), 501–510. doi:10.1109/TFUZZ.2014.2315661

Zhou, Q., Li, H., Wu, C., Wang, L., & Ahn, C. K. (2017). Adaptive fuzzy control of nonlinear systems with unmodeled dynamics and input saturation using small-gain approach. *IEEE Transactions on Systems Man & Cybernetics Systems*, 47(8), 1979–1989. doi:10.1109/TSMC.2016.2586108

Zhu, M., & Li, Y. (2010). Decentralized adaptive fuzzy sliding mode control for reconfigurable modular manipulators. *International Journal of Robust and Nonlinear Control: IFAC-Affiliated Journal*, 20(4), 472–488. doi:10.1002/rnc.1444

Appendix

The Coriolis matrix $C(\dot{q}, q)$ in Equation (1) is:

$$C(\dot{q}, q) = \begin{bmatrix} c_{11} & c_{12} & c_{13} \\ c_{21} & c_{22} & c_{23} \\ c_{31} & c_{32} & c_{33} \end{bmatrix}$$

with the elements are:

$$\begin{aligned}
c_{11} &= (J_1 \cos\beta \sin\beta \cos^2\gamma - J_2 \cos\beta \sin\beta \sin^2\gamma \\
&\quad + J_3 \sin\beta \cos\beta)\dot{\beta} + (-J_1 \sin\gamma \cos\gamma \cos^2\beta \\
&\quad + J_2 \cos^2\beta \sin\gamma \cos\gamma)\dot{\gamma}
\end{aligned}$$

$$\begin{aligned}
c_{12} &= (-J_1 \cos\beta \sin\beta \cos^2\gamma - J_2 \cos\beta \sin\beta \sin^2\gamma \\
&\quad + J_3 \sin\beta \cos\beta)\dot{\alpha} + ((J_1 - J_2) \sin\beta \sin\gamma \cos\gamma)\dot{\beta} \\
&\quad + \frac{1}{2}(-(J_1 - J_2) \cos\beta \sin^2\gamma \\
&\quad + (J_1 - J_2) \cos\beta \cos^2\gamma + J_3 \sin\beta)\dot{\gamma}
\end{aligned}$$

$$\begin{aligned}
c_{13} &= -((J_1 - J_2) \cos\gamma \sin\gamma \cos^2\beta)\dot{\alpha} \\
&\quad + \frac{1}{2}(-(J_1 - J_2) \cos\beta \sin^2\gamma \\
&\quad + (J_1 - J_2) \cos\beta \cos^2\gamma + J_3 \cos\beta)\dot{\beta}
\end{aligned}$$

$$\begin{aligned}
c_{21} &= (J_1 \cos\beta \sin\beta \cos^2\gamma + J_2 \cos\beta \sin\beta \sin^2\gamma \\
&\quad - J_3 \sin\beta \cos\beta)\dot{\alpha} + \frac{1}{2}(-(J_1 - J_2) \cos\beta \sin^2\gamma \\
&\quad + (J_1 - J_2) \cos\beta \cos^2\gamma - J_3 \cos\beta)\dot{\gamma}
\end{aligned}$$

$$c_{22} = ((J_1 - J_2) \cos\gamma \sin\gamma)\dot{\gamma}$$

$$\begin{aligned}
c_{23} &= \frac{1}{2}(-(J_1 - J_2) \cos\beta \sin^2\gamma \\
&\quad + (J_1 - J_2) \cos\beta \cos^2\gamma - J_3 \cos\beta)\dot{\alpha} \\
&\quad + ((J_1 - J_2) \cos\gamma \sin\gamma)\dot{\beta}
\end{aligned}$$

$$\begin{aligned}
c_{31} &= ((J_1 - J_2) \cos\gamma \sin\gamma \cos^2\beta)\dot{\alpha} + \frac{1}{2}((J_1 - J_2) \cos\beta \sin^2\gamma \\
&\quad - (J_1 - J_2) \cos\beta \cos^2\gamma - J_3 \cos\beta)\dot{\beta}
\end{aligned}$$

$$\begin{aligned}
c_{32} &= \frac{1}{2}((J_1 - J_2) \cos\beta \sin^2\gamma \\
&\quad - (J_1 - J_2) \cos\beta \cos^2\gamma + J_3 \cos\beta)\dot{\alpha} \\
&\quad - ((J_1 - J_2) \cos\gamma \sin\gamma)\dot{\beta}
\end{aligned}$$

$$c_{33} = 0.$$